Reduced Rib Synchronous Reluctance Motor for Traction Applications

Sibasish PANDA, Ritesh Kumar KESHRI
Visvesvaraya National Institute of Technology, Department of Electrical Engineering
Nagpur, 440010, India
sibasispanda@students.vnit.ac.in, *riteshkeshri@ieee.org*

***Abstract*—This paper proposes a variable width reduced rib rotor structure for Synchronous Reluctance (SynRel) Motor. In convention supporting iron ribs are introduced in transversally laminated anisotropic (TLA) type rotors of SynRel motor to increase the robustness of the rotor structure for high speed operations. However, the presence of these ribs degrades the electromagnetic performance of the motor such as saliency ratio and average output torque due to the flux path oriented along q-axis, through the rib area. Hence, the selection of appropriate shape and number of support ribs are essential to ensure the robustness of the rotor without much affecting the required torque density. Present paper uses Finite Element Analysis (FEA) to study electromagnetic as well as mechanical performance of SynRel motor. Rotor structure employing variable width for radial ribs is proposed. The use of variable width in radial ribs decrease the inductance oriented along q-axis, thus improving the saliency ratio and average output torque of SynRel motor. A 1 kW prototype is fabricated for the proposed rotor structure. A detailed comparison between the conventional and proposed rotor structure is also presented to demonstrate the advantages of the latter for high speed and high torque density applications.**

***Index Terms*—AC machines, finite element analysis, rotors, stress measurement, traction motor.**

I. Introduction

High efficiency, low torque ripple, low acoustic noise, high torque density and high reliability are considered to be the major requirements of electric motor for traction applications [1]. Permanent Magnet Synchronous Motor (PMSM) and Induction Motor (IM) are in use for the last few decades for traction applications [2-4] owing to their advantages such as high torque density and low torque ripple in PMSMs and high reliability in IMs. However, the fluctuating price of rare-earth magnets and rotor copper loss issues lead the automotive industries and researchers to explore the possibilities of permanent-magnet-free motors [5].

Synchronous reluctance (SynRel) motor is considered to be a suitable competitor to PMSM and IM. The elimination of rotor winding allows SynRel to be low cost and highly efficient compared to IM. Although, SynRel is as old as IM [6] it is often ignored because of its relatively complicated rotor structure. The rotor is manufactured using axially laminated magnetic material layers separated by non-magnetic barriers as shown in Fig. 1a, which makes the manufacturing process more complicated and expensive [7-8]. The use of transversely laminated rotor [9] makes the design process simpler. It uses traditional die cut or laser cut process to cut the laminations, each of thickness around 0.35 mm to 0.5 mm as illustrated in Fig. 1b. In spite of the better manufacturability, transversally laminated rotor suffers from low saliency ratio. The presence of radial and tangential ribs increases the inductance along q-axis, thus decreasing the saliency ratio and average output torque. However, these ribs are necessary since they provide mechanical strength to the rotor structure. An enormous effort has been recently made to increase the saliency ratio of transversally laminated rotors [10-11]. In [12-14], the authors focused on the shape of barriers to enhance the torque performance of SynRel. The torque density of SynRel can be improved by introducing low cost ferrite magnets inside the flux barriers however, the torque performance depends on the location and size of these magnets [15].

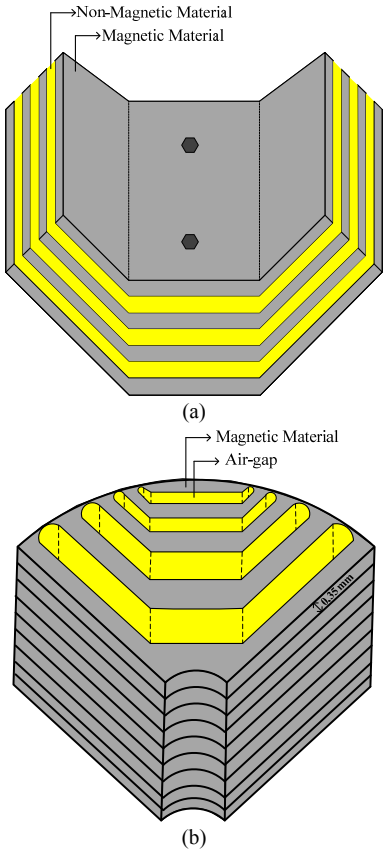

Figure 1. Rotor designs of SynRel (a) axially laminated (b) transversely laminated.

Furthermore, the anisotropic structure makes SynRel to be an erroneous choice for high speed operation. This is due to the rotational forces acting on the rotor structure exceeds the maximum stress limit of the core material. For

This work is supported by Department of Science & Technology and Ministry of Electronics and Information Technology, Government of India.

Digital Object Identifier 10.4316/AECE.2019.04010

transversally laminated anisotropic (TLA) type rotor these forces are maximum at the tangential and radial rib area and depends on the width of these ribs i.e., wider ribs makes the rotor more robust. However, wider ribs degrades the output torque of SynRel because of decrease in saliency ratio. Hence, the sizing of these ribs are quite essential both from electromagnetic and mechanical performance point of view.

In [16], the authors proposed the analysis between various rotor models with radial and tangential ribs of distinct widths. However, the width of radial ribs are maintained constant for each barrier segment. Furthermore, a new rib structure is proposed in [17] for high speed and high power applications. This paper presents the effects of tangential and radial ribs for high speed operation. The sizing of these ribs are done by taking the mutual effects of electromagnetic and mechanical performance of SynRel. To increase the torque performance of SynRel, radial ribs with variable width (parabolic structure) is proposed. A prototype is fabricated and the comparative analysis is carried out between the conventional and the proposed SynRel, to validate the advantages of proposed rotor structure over the existing one.

II. ANALYSIS

The operating principle of SynRel is same as the operation of salient pole synchronous motor with field winding unexcited. Fig. 2a shows the two-dimensional view of the stator, rotor and windings, while the complete three-dimensional view from Ansys Maxwell is presented in Fig. 2b. Owing to its anisotropy in the structure, the stator flux oriented along q-axis flows through a high reluctance path and the flux component along d-axis follows a low reluctance path. Torque is produced because of the tendency of the rotor to reach the position for which the overall reluctance of the stator flux path is minimum. The reluctance torque is expressed in (1).

$$T_e = \frac{3}{2} P_0 L_d \left(1 - \frac{1}{\xi}\right) I_d I_q \tag{1}$$

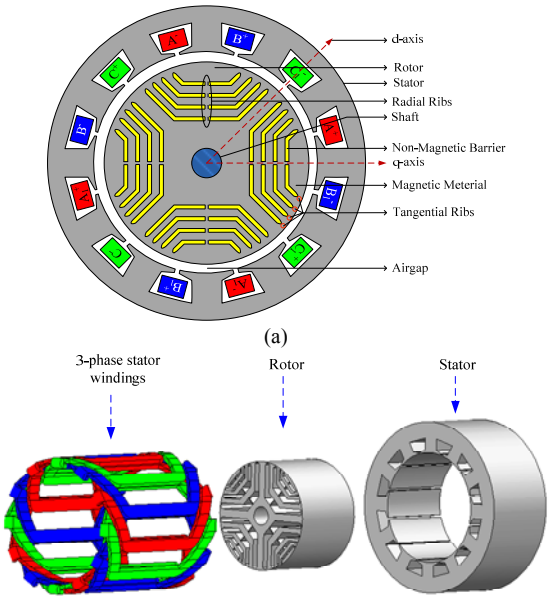

Figure 2. General representation of 4-pole SynRel (a) 2D-view (b) 3D-view.

where, P_0 is the number of pole pairs, L_d is the inductance along d-axis, ξ is the saliency ratio, I_d and I_q are the current components along d-axis and q-axis, respectively. It is evident that, the electromagnetic torque is dependent on the saliency ratio (ξ) which is given by the ratio of direct to quadrature axis inductance as expressed in (2).

$$\xi = \frac{L_d}{L_q} \tag{2}$$

Direct axis and quadrature axis inductances depend upon the design of the rotor structure i.e., different anisotropy structure produces different values for L_d and L_q. Hence, torque performance of SynRel can be improved by improving the saliency ratio of the motor i.e., L_d has to be high and L_q has to be as low as possible. Further, in reluctance motors the flux linkage changes with respect to the change in rotor angle. Thus, the flux density distribution do not have constant wave shape around the air-gap. Consequently, these inductances can be calculated from the MMF distribution. The detailed calculation of inductances from the motor geometry are quite complex and are reported in [18]. In this paper, the d and q-axes inductances are calculated from the characteristics of self and mutual inductance (ref. Fig. 3), obtained from FEA, and are given by (3)-(4) [19-20].

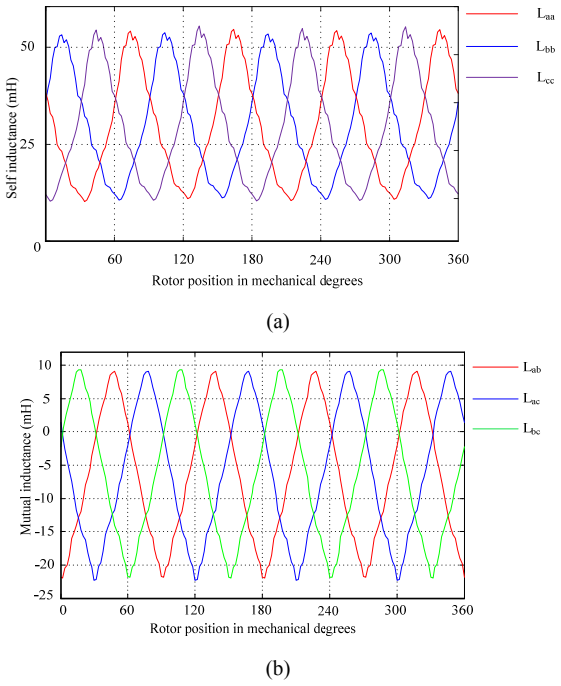

Figure 3. Variation of (a) self-inductance (b) mutual-inductance, with rotor position in mechanical degrees.

$$L_d = L_l + \frac{3}{2}\left(L_{av} + L_{sh}\right) \tag{3}$$

$$L_q = L_l + \frac{3}{2}\left(L_{av} - L_{sh}\right) \tag{4}$$

where, L_l is the phase leakage inductance, L_{av} is the average component of self-inductance and L_{sh} is the magnitude of second harmonic component.

The power factor (*p.f*) of SynRel is also affected by the values of L_d and L_q and is presented in (5), while the maximum *p.f* is presented in (6).

$$\cos\phi = \frac{(\xi - 1) I_d I_q}{\left(\sqrt{(\xi I_d)^2 + I_q^2}\right)\left(\sqrt{I_d^2 + I_q^2}\right)} \quad (5)$$

$$\cos\phi_{\max} = \frac{\xi - 1}{\xi + 1} \quad (6)$$

The parameters considered for the design purpose are illustrated in Table I. Since the overall performance of SynRel is highly influenced by ξ, hence the primary design goal is to maximize the value of ξ. In order to maximize ξ, which further depends on the inductances of the machine, the width of flux barriers and carriers should be optimized. The selection of the width of barriers and carriers are presented in the following subsection.

TABLE I. DESIGN SPECIFICATIONS

Symbol	Parameter	Value
P_n	Output power	1 kW
T_e	Electromagnetic torque	6 Nm
N_b	Base speed	1500 rpm
P_0	Pole pairs	2
m	Number of phases	3
N_S	Number of stator slots	12
l_g	Length of airgap	0.3 mm
D_{so}	Stator outer diameter	137 mm
L	Stack length	60 mm
q	Slots per pole per phase	1

A. Selection of Barriers and Carriers

Since the rotor's anisotropic structure affects the electromagnetic torque, the selection of the width of barriers and carriers plays a vital role in the design process. The effect of the number of barriers is already discussed in [14], [21]. Fig. 4 shows the dimensional details of the rotor structure. The width of barriers and carriers are computed by considering two factors i.e., insulation ratio K_q along q-axis and MMF distribution along d and q-axes, respectively. K_q can be defined as the ratio of total air to total iron oriented along q-axis and is given by (7). The width of barriers and carriers are obtained using (8)-(9) and the detail concepts of these equations are presented in [13].

$$K_q = \frac{l_g + \sum_{u=1}^{x} B_u}{\frac{D_{ro}}{2} - \frac{D_{ri}}{2} - \sum_{u=1}^{x} B_u} \quad (7)$$

where, D_{ro} is the outer diameter of the rotor, D_{ri} is the inner diameter of the rotor, B stands for barrier, l_g is the length of airgap between the stator and the rotor and x is total number of barriers.

$$\frac{B_u}{B_v} = \left(\frac{\Delta f_u}{\Delta f_v}\right)^2 \quad u \text{ and } v = 1,2, \ldots, x. \quad (8)$$

where, u and v are the barrier numbers and $u \neq v$ and Δf_u is the difference in MMF of barrier u, when q-axis MMF is applied to the motor.

$$\frac{C_u}{C_v} = \frac{f_{du}}{f_{dv}} \quad u \text{ and } v = 1,2, \ldots, x+1. \quad (9)$$

where, u and v are the carrier numbers and $u \neq v$ and f_{du} is the average MMF in the carrier u, when d-axis MMF is applied to the motor and x+1 is the total number of carriers in the rotor geometry.

The variation of inductances along d and q-axes with insulation ratio is illustrated in Fig. 5a, while Fig. 5b shows the characteristics of average electromagnetic torque (T_{avg}) and saliency ratio (ξ) with the variation in insulation ratio. As discussed earlier, for each value of K_q, L_d and L_q are calculated on the basis of the self and mutual inductances obtained from FEA. It can be observed from Fig. 5b that, for $0.2 \leq K_q < 0.6$, there is a healthy improvement in T_{avg} due to the introduction of airgap. The increment in airgap creates a high reduction in L_q as shown in Fig. 5a whereas, L_d remains

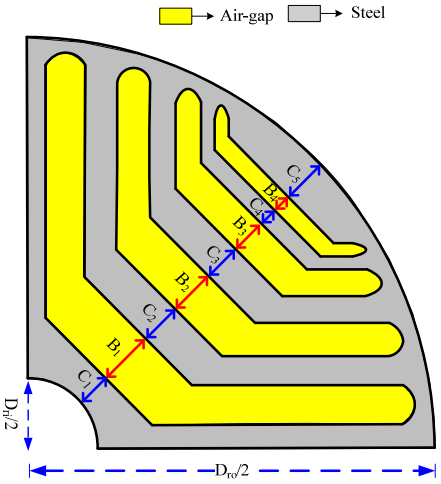

Figure 4. Single pole geometry of rotor structure.

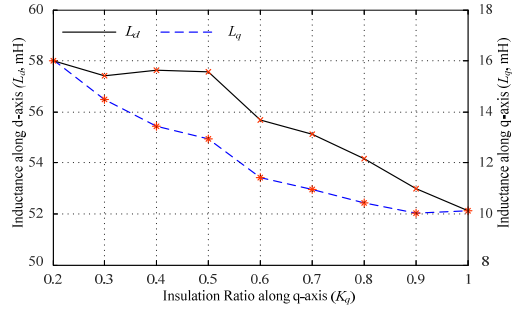

(a)

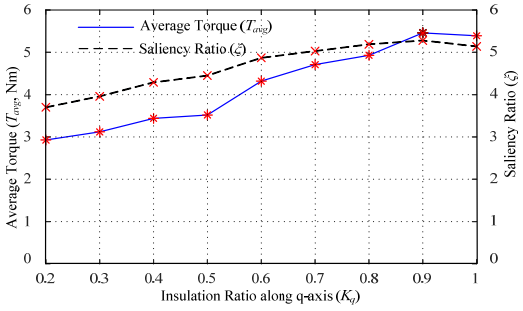

(b)

Figure 5. Impact of insulation ratio on (a) L_d and L_q (b) T_{avg} and ξ.

TABLE II. SPECIFICATIONS OF ROTOR GEOMETRY FOR $K_q = 0.85$

Parameter	Symbol	Value (mm)
Rotor outer diameter	D_{ro}	87.1
Rotor inner diameter	D_{ri}	15
Stack length	L	60
Carrier-1	C_1	5
Carrier-2	C_2	5.38
Carrier-3	C_3	3.7
Carrier-4	C_4	2.77
Carrier-5	C_5	2.8
Barrier-1	B_1	6.5
Barrier-2	B_2	5.26
Barrier-3	B_3	2.6
Barrier-4	B_4	2.05

almost constant. For $0.6 \leq K_q < 0.8$, there is not much variation in the torque because L_q has already approached to its minimum value and further decreases slowly. For $0.8 \leq K_q < 0.9$, optimal results are obtained considering average torque and saliency ratio. For $K_q \geq 0.9$, there is further increment in airgap and decrement in steel which in turn, reduces T_{avg} due to the decrement in L_d and L_q has already approached to its minimum level. Present design uses $K_q = 0.85$, and the detail width of barriers and carriers are summarized in Table II.

III. Electromagnetic and Structural Analyses (FEA-3D)

The rotor dimensions obtained from previous section undergoes electromagnetic and structural analyses for high speed operation. The presence of anisotropy in the rotor structure, limits the high speed operation of SynRel. At high speed, rotational forces are quite dominant on the rotor geometry and may create unwanted deformation at the critical joints such as tangential and radial rib area. Generally, SynRel is equipped with a small airgap between the stator and rotor, for present design it is 0.3 mm therefore, it is quite essential to perform the structural analysis along with electromagnetic analysis on the rotor geometry. Hence, the model from Ansys Maxwell-3D undergoes structural analysis using Ansys Workbench (static structural-3D) mainly to evaluate maximum principal stress acting on the rotor and the total deformation of the rotor geometry. The simultaneous effects of electromagnetic and structural analyses for various size and shape of ribs are discussed in the following subsections.

A. Effect of Tangential Ribs

From the electromagnetic point of view the width of tangential ribs considered to be as thin as possible, owing to its advantage of decrement in q-axis flux and L_q. The torque loss due to tangential ribs is given by (10) [22].

$$T_{loss} = \frac{16P_0^2}{\mu_0} W_r l B_r B_d K_c l_g K_s \tag{10}$$

where, W_r is the width of tangential rib, l is the thickness of laminations, B_r is the maximum rib flux density, P_0 is the number of pole pairs, B_d is the d-axis flux density, l_g is the length of air gap, K_c is the Carter factor and K_s is the saturation factor. In (10), assuming all other parameters to be constant, it can be observed that, the torque loss is a function of tangential rib width. Thus, to obtain improved torque performance it is quite recommended to reduce the thickness of tangential ribs. However, the decrement in the width of these ribs beyond a certain limit is not advisable owing to the fact that, it has an adverse effect on the structural performance of the motor. Hence, the selection of these ribs are carried out by performing electromagnetic and structural analyses simultaneously, with W_r varies from 0.4 mm to 1 mm as illustrated in Fig. 6. The rotor structure with $W_r < 0.4$ mm is not considered for the purpose of analysis owing to its complexity in manufacturing.

Fig. 7a shows the variation of L_d and L_q for the variation in W_r. A distinct variation of L_q is observed as a consequence of the change in W_r. L_q is increased by 27.18% for rib width of 1 mm from its initial value of 0.4 mm, while the variation of W_r has a minor impact on L_d. This increase in L_q makes the ξ of SynRel poor, which in turn degrades the torque performance of the motor and is illustrated in Fig. 7b. For an increase of 0.1 mm in rib width i.e., from 0.4 mm to 0.5 mm the average torque is reduced by 2.37% with respect

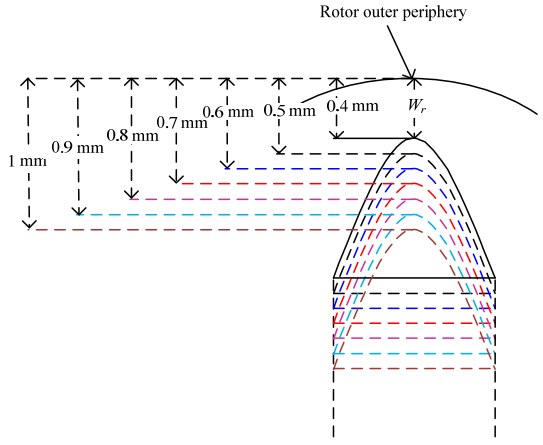

Figure 6. Layout for the width of tangential ribs for 0.4 mm ≤ W_r ≤ 1 mm.

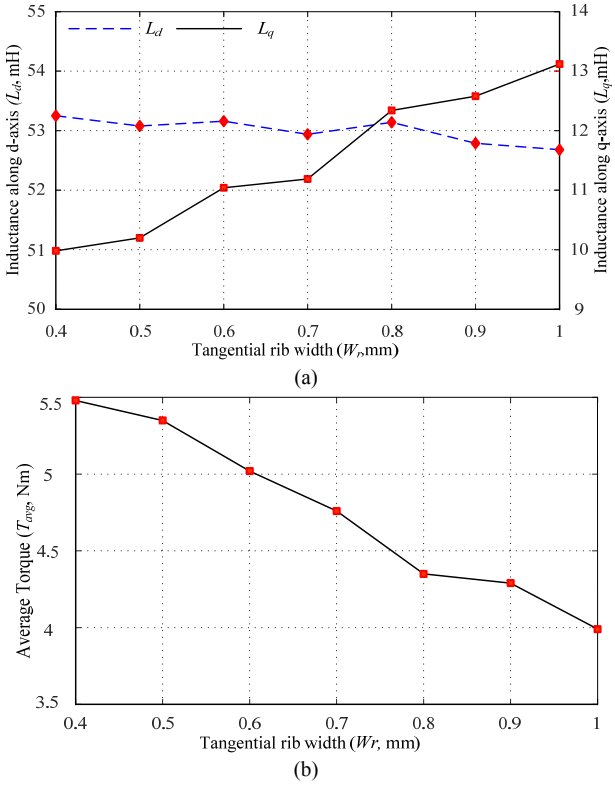

Figure 7. Impact of tangential rib width (W_r) on (a) L_d and L_q (b) T_{avg}.

to the prior one, while a reduction of 8.39%, 13.13%, 20.62%, 21.71% and 27.18% is observed for rib width of 0.6 mm, 0.7 mm, 0.8 mm, 0.9 mm and 1 mm, respectively as presented in Table III.

TABLE III. Electromagnetic Performance of SynRel for, 0.4 mm ≤ W_r ≤ 1 mm

W_r (mm)	ξ	T_{avg} (Nm)
0.4	5.33	5.48
0.5	5.20	5.35
0.6	4.81	5.02
0.7	4.73	4.76
0.8	4.30	4.35
0.9	4.19	4.29
1	4.01	3.99

Thus, from electromagnetic performance point of view

the tangential ribs should be as narrow as possible. However, again narrow ribs increase the maximum stress and leads to the formation of fatigue on the rotor structure. The maximum stress sustained by the core material is presented in Table IV (ThyseenKrupp data sheet). For the reliable operation of SynRel at high speed, it is always desired to have a safety factor for stress, present design uses a safety factor of 1.5. Thus, with safety factor of 1.5, the stress at which the core material starts deforming (yield stress) is 213 Mpa and it breaks permanently (tensile stress) at 300 Mpa.

TABLE IV. SPECIFICATIONS OF M19

Parameter	Value
Yield stress	320 Mpa
Tensile stress	450 Mpa
Poisson's ratio	0.27

The maximum stress and deformation is evaluated by FEA-3D for 6000 rpm and the results are presented in Table V. It can be observed from the stress analysis that, the maximum stress decreases with the increase in W_r. The percentage reduction in stress and deformation for different rotor structures with respect to the rotor with $W_r = 0.4$ mm is illustrated in Fig. 8.

TABLE V. STRUCTURAL PERFORMANCE OF SYNREL FOR, 0.4 MM ≤ W_r ≤ 1 MM

W_r (mm)	Maximum principal stress (Mpa)	Maximum deformation (μm)
0.4	353.72	58.01
0.5	292.67	55.60
0.6	248.32	54.04
0.7	213.87	52.71
0.8	187.33	51.71
0.9	173.76	50.91
1	170.90	50.22

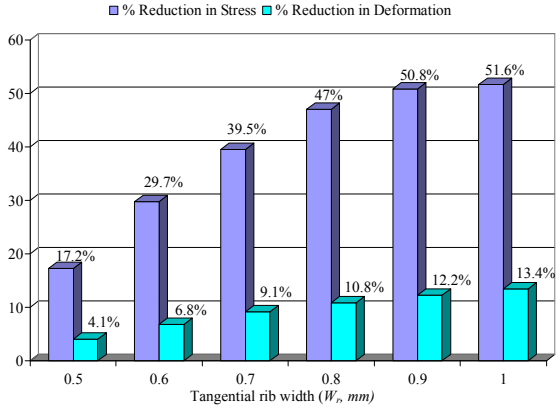

Figure 8. Percentage reduction in maximum stress and deformation.

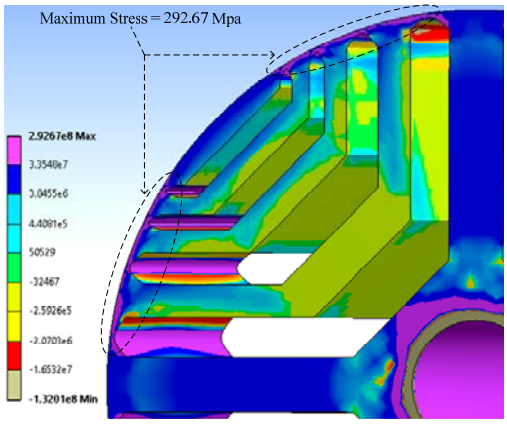

Figure 9. Maximum principal stress for $W_r = 0.5$ mm, at 6000 rpm.

Hence, to meet the critical limit of 213 Mpa, the rotor structure with $W_r = 0.7$ mm should be adopted. However, from the electromagnetic point of view with $W_r = 0.7$ mm, the average torque is reduced by 13.13% with respect to the design with $W_r = 0.4$ mm. For $W_r = 0.4$ mm, the stress developed is beyond the actual yield stress limit of the core material thus, 0.4 mm tangential rib width cannot be selected for final design.

Therefore, the rotor design with $W_r = 0.5$ mm is selected, where the stress is lower than the actual yield stress limit of the core material as illustrated in Fig. 9, with a penalty in average torque of 2.37%. However, the goal of 213 Mpa (critical stress limit with safety factor of 1.5) is not achieved with $W_r = 0.5$ mm. Hence, the rotor is provided with some additional supports called radial ribs (R_r) to meet the critical limit of 213 Mpa and is discussed in the following subsection.

B. Effect of Radial Ribs

The prior discussion concludes that, with wider tangential rib the electromagnetic performance decreases but mechanical integrity increases. Since, the electromagnetic performance of SynRel is quite sensitive to tangential rib width a little increase in W_r results an immense loss in T_{avg} Therefore, radial ribs are provided to increase the robustness of SynRel for high speed operation. Fig. 10a and Fig. 10b shows the conventional structures with 0.5 mm and 1 mm ribs, respectively [23].

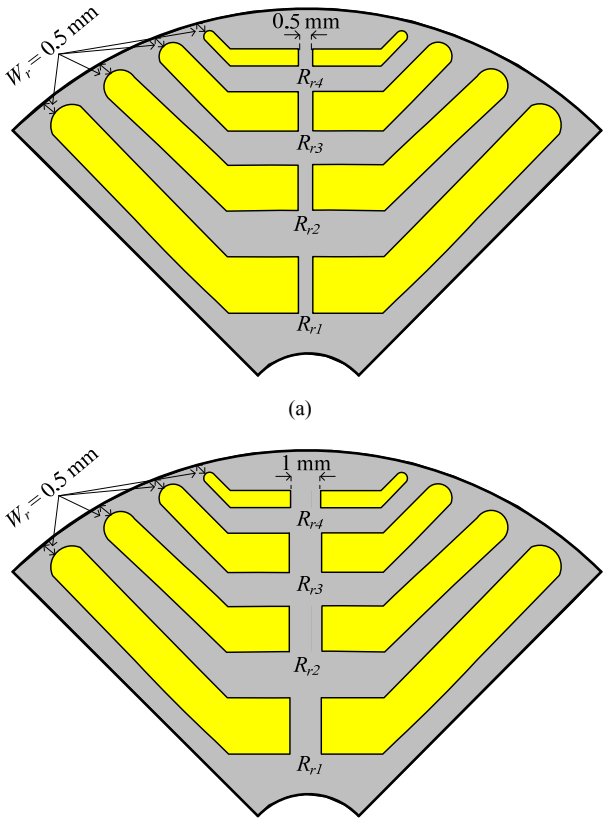

Figure 10. Conventional rotor geometry with (a) 0.5 mm radial rib (Type-A). (b) 1 mm radial rib (Type-B).

The introduction of radial ribs improves the stress profile of the system but at the same time, it provides an additional path for q-axis flux, which further decreases ξ and T_{avg}.

Thus, it is very important to size and place the radial ribs at appropriate location. Fig. 11a and Fig. 11b shows the stress analysis of different conventional structures, where along with tangential ribs, radial ribs of 0.5 mm (Type-A) and 1 mm (Type-B) are also introduced. After the introduction of radial ribs, it can be observed from FEA that, for Type-A the stress level drops down to 238 Mpa from 292.67 Mpa. However, the critical value of 213 Mpa (with safety factor of 1.5) is not achieved for Type-A. Further, the stress analysis is performed on Type-B, where the stress level drops down to 165.89 Mpa from 292.67 Mpa as presented in

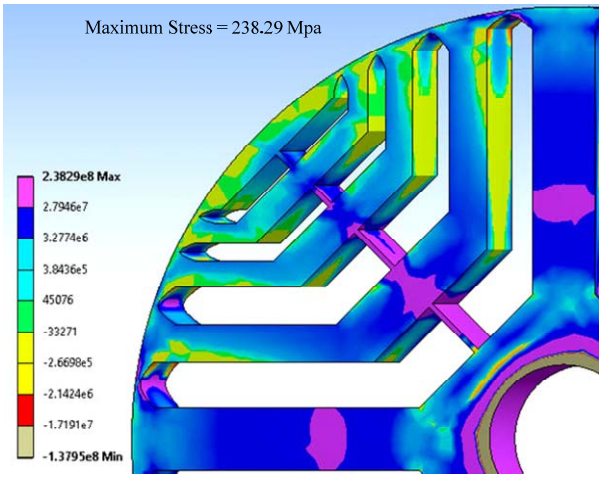

(a)

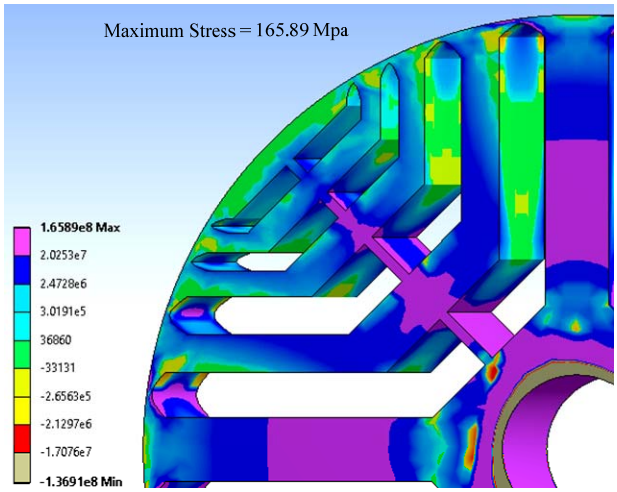

(b)

Figure 11. Maximum principal stress at 6000 rpm. (a) Type-A. (b) Type-B.

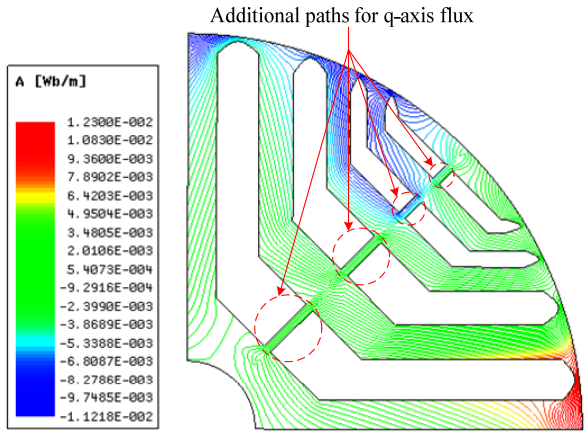

Figure 12. Magnetic flux lines distribution for Type-B.

Fig. 11b, which is below the critical limit of 213 Mpa. But at the same time electromagnetic analysis is also necessary since radial ribs provide additional path for q-axis flux and is shown in Fig. 12. For Type-B, T_{avg} drops to 4.53 Nm from 5.35 Nm (without radial ribs and W_r = 0.5 mm). Hence, to improve the electromagnetic performance of SynRel the shape of radial ribs are modified, and the detail analysis is presented in next section.

IV. Proposed Geometry with Variable Radial Rib Width

To meet the stress limit of the core material with safety factor of 1.5, radial ribs are provided in the rotor geometry. Two rotor structures with different rib width i.e., 0.5 mm (Type-A) and 1 mm (Type-B) are discussed in detail. Type-A is not found suitable since the stress developed is beyond the critical limit of the core material at high speed operation. While, Type-B is found suitable for high speed operation, where the stress developed is within the safe limit of the core. However, because of the introduction of wider radial ribs the torque loss increases due to the increase in q-axis flux as illustrated in Fig. 12. Hence, it is necessary to redesign the rib geometry, which will lead to the minimization of torque loss with acceptable stress.

This section presents the detail analyses of radial ribs with variable rib width. The proposed radial rib (Type-C) is shown in Fig. 13, where the contact point with the carrier is wider than the central width. The main reason to choose this type of structure is to ensure the mechanical strength at high speed and to minimize the loss in the average torque. The narrow central width of the ribs reduces the flow of q-axis flux, consequently, there is a decrease in L_q and increase in T_{avg}. On the other hand, the wider rib openings at the contact point with the carriers provides good mechanical strength to the rotor at high speed operation.

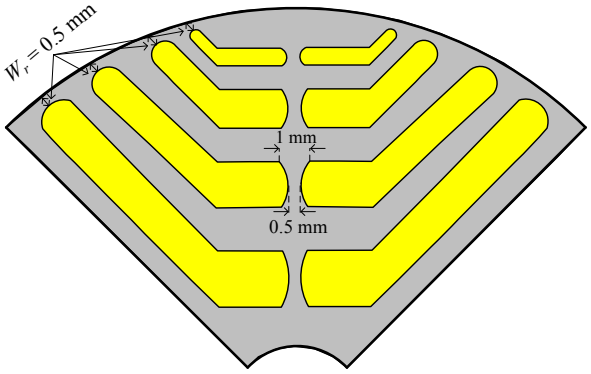

Figure 13. Initial geometry of the proposed rotor structure with variable radial rib width (Type-C).

Fig. 14 shows the stress analysis of the proposed rotor structure. It is evident to note that, the maximum stress developed because of the rotational forces is maintained under the critical limit of the core material. The radial ribs near the outer periphery of the rotor i.e., R_{r4} and R_{r3} are lightly stressed thus these ribs can be removed from the final structure. In addition to this, the stress level of radial ribs R_{r1} and R_{r2} is 189.75 Mpa, while the stress level of tangential ribs are 22.82 Mpa this shows an unequal stress distribution between the ribs.

Fig. 15 shows the final rotor structure (Type-D). The two

outer most radial ribs are removed from the rotor and stress analysis is performed again, which is illustrated in Fig. 16a. The maximum stress developed by the final structure (Type-D) is 175.16 Mpa, which is within the safe limit of core material and stress is equally distributed between the radial and tangential ribs. Fig. 16b shows the deformation profile of the final proposed rotor, which is also within the acceptable range. Electromagnetic analysis is also carried out on the proposed Type-D rotor simultaneously. Table VI summarizes a detail comparison between SynRels with conventional (Type-B) and proposed (Type-D) rotor structures. Fig. 17 shows the actual fabricated rotor structure for Type-D.

The maximum stress for conventional (Type-A and Type-B) and proposed (Type-D) with the variation in rotor speed is illustrated in Fig. 18, while Fig. 19 shows the torque angle characteristics for SynRels with conventional (Type-B) and proposed (Type-D) rotor structures. An increment of 7.5% in T_{avg} is recorded in the proposed rotor structure (Type-D) over the conventional structure (Type-B). Furthermore, the stress developed by Type-D is 17.76% lower than the critical limit of the core material.

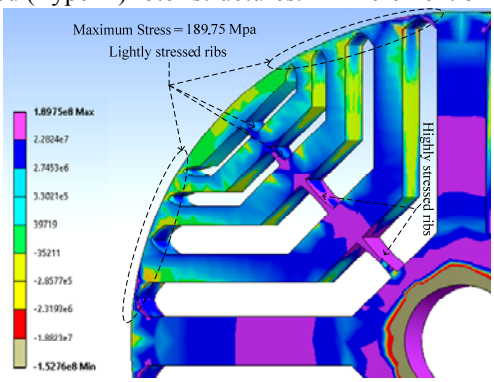

Figure 14. Maximum principal stress for Type-C at 6000 rpm.

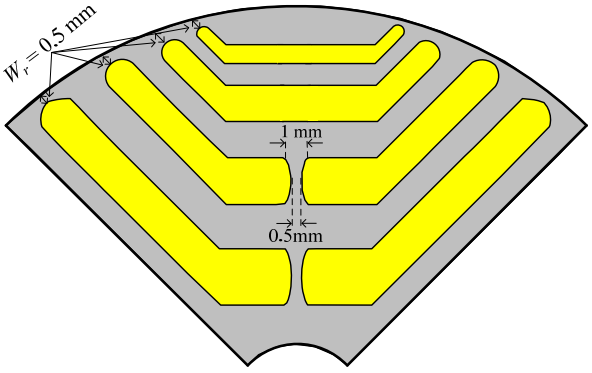

Figure 15. Final geometry of the proposed rotor structure with variable radial rib width (Type-D).

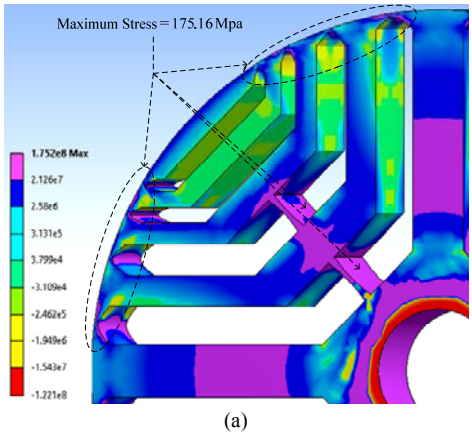

(a)

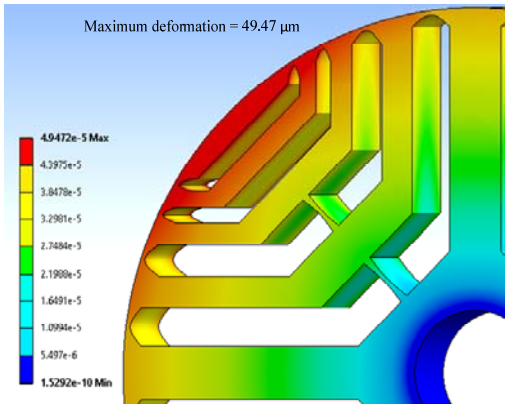

(b)

Figure 16. (a) maximum principal stress for Type-D at 6000 rpm (b) maximum deformation of Type-D at 6000 rpm.

TABLE VI. COMPARISON OF PROPOSED SYNREL DESIGN WITH CONVENTIONAL DESIGN

Parameter	Conventional (Type-B)	Proposed (Type-D)
Average torque (T_{avg} Nm)	4.53	4.87
Saliency ratio (ξ)	4.41	4.93
Efficiency (%η)	90.35	92.57
Active mass of rotor (grams)	1579.6	1563.5
Maximum stress (Mpa)	165.89	175.16
Total deformation (µm)	44.02	49.47

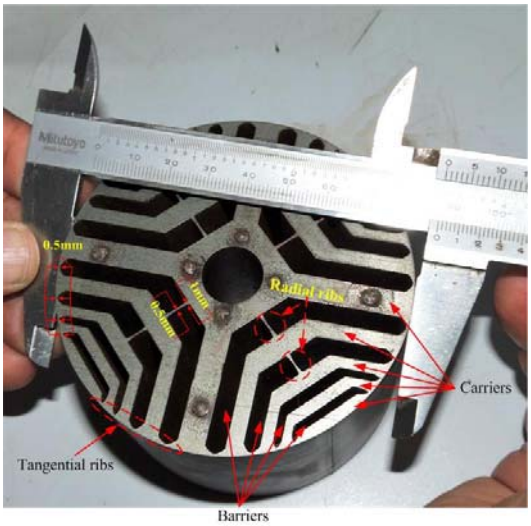

Figure 17. Final fabricated rotor geometry (Type-D).

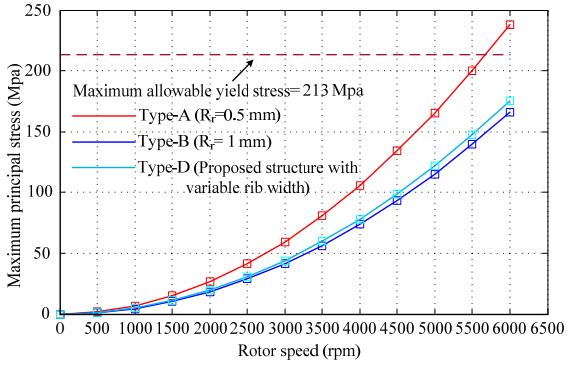

Figure 18. Characteristics of maximum stress with variation in rotor speed.

Thus, from the comparative analysis it can be concluded that, the proposed rotor structure with variable radial ribs is

not only advantageous in terms of torque performance but also mechanically robust and suitable for high speed and high torque density applications. However, for high power and high speed (18000 rpm) applications the rib structure presented in [17] claimed an increase of 65% power at high speed operation with respect to conventional structure. But at the same time it increases the complexity in fabrication further increasing its production cost and will be suitable for heavy electric vehicle applications. Hence, the proposed rotor structure (Type-D) is advantageous and cost effective for low power and light electric vehicle applications.

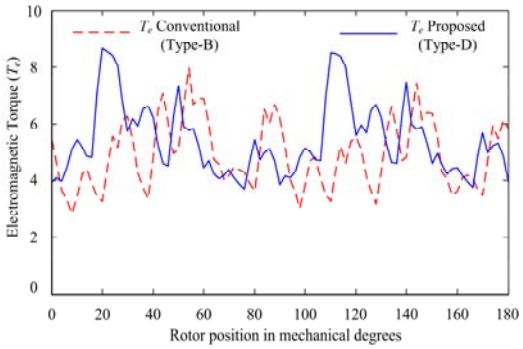

Figure 19. Torque angle characteristics of SynRel for Type-B and Type-D rotor.

V. Conclusion

For automotive applications, the design of rotor structure for SynRel equipped with transversally laminated rotor is studied in detail. The width of barriers and carriers are computed by considering two factors i.e., insulation ratio and MMF distribution along d and q-axes, respectively. The effect of insulation ratio varying from 0.2 to 1, on saliency ratio and average torque are also discussed. The insulation ratio with 0.85 is found acceptable when average torque and saliency ratio are considered. To ensure the reliable operation of the motor at high speed, magnetic FEA-3D is assisted by mechanical FEA-3D to evaluate the stress and total deformation profile of the rotor. The effects of the width of the radial and tangential ribs are also presented from both electromagnetic and mechanical performance point of view. From the simultaneous analysis on both electromagnetic and mechanical performance it is concluded that, electromagnetic performance and mechanical robustness of SynRel are the two sides of a coin. This means electromagnetic performance can be increased by degrading the mechanical robustness of the rotor structure and vice versa. Hence, the radial ribs are redesigned utilizing variable width at different locations. The introduction of variable rib width increases the average torque by 7.5% with respect to conventional structure (Type-B). The proposed structure (Type-D) is also found to be mechanically robust enough and is within safe stress limit of 17.76% of the core material.

References

[1] C. C. Chan, "The state of the art of electric and hybrid vehicles," Proc. IEEE, vol. 90, no. 2, pp. 247–275, Feb. 2002, doi:10.1109/5.989873.

[2] M. Aktas, "A Novel Method for Inverter Faults Detection and Diagnosis in PMSM Drives of HEVs based on Discrete Wavelet Transform," Advances in Electrical and Computer Engineering, vol.12, no.4, pp.33-38, 2012, doi:10.4316/AECE.2012.04005

[3] A. Simion, L. Livadaru, S. Mihai, A. Munteanu, C. G. Cantemir, "Induction Machine with Improved Operating Performances for Electric Trucks. A FEM-Based Analysis," Advances in Electrical and Computer Engineering, vol.10, no.2, pp.71-76, 2010, doi:10.4316/AECE.2010.02012

[4] P. Palacky, P. Brandstetter, P. Chlebis, V. Sladecek, P. Simonik, D. Slivka, "Control Algorithms of Propulsion Unit with Induction Motors for Electric Vehicle," Advances in Electrical and Computer Engineering, vol. 14, no. 2, pp.69-76, 2014, doi:10.4316/AECE.2014.02012

[5] I. Boldea, L. N. Tutelea, L. Parsa and D. Dorrell, "Automotive Electric Propulsion Systems With Reduced or No Permanent Magnets: An Overview," IEEE Trans. on Ind. Electron., vol. 61, no. 10, pp. 5696-5711, Oct. 2014, doi:10.1109/TIE.2014.2301754.

[6] J. K. Kostko, "Polyphase reaction synchronous motors," J. Amer. Inst. Elect. Eng., vol. 42, pp. 1162–1168, 1923, doi:10.1109/JoAIEE.1923.6591529.

[7] E. S. Obe, "Calculation of inductances and torque of an axially laminated synchronous reluctance motor," IET Electric Power Applications, vol. 4, no. 9, pp. 783-792, Nov. 2010, doi:10.1049/iet-epa.2009.0197.

[8] E. K. Beser, S. Camur, B. Arifoglu, E. Beser, "Design and Analysis of an Axially Laminated Reluctance Motor for Variable-Speed Applications," Advances in Electrical and Computer Engineering, vol.13, no.1, pp.75-80, 2013, doi:10.4316/AECE.2013.01013.

[9] C. Liu, T. Luo, C. Hwang and B. Chang, "Field Path Design Assessments of a High-Performance Small-Power Synchronous-Reluctance Motor," IEEE Trans. on Magn., vol. 51, no. 11, pp. 1-4, Nov. 2015, Art no. 8206504, doi:10.1109/TMAG.2015.2443831.

[10] D. A. Staton, T. J. E. Miller and S. E. Wood, "Maximising the saliency ratio of the synchronous reluctance motor," IEE Proc. B Electr. Power Appl., vol. 140, no. 4, pp. 249-259, July 1993, doi:10.1049/ip-b.1993.0031.

[11] C. M. Donaghy-Spargo, "Electromagnetic–Mechanical Design of Synchronous Reluctance Rotors With Fine Features," IEEE Trans. on Magn., vol. 53, no. 11, pp. 1-8, Nov. 2017, Art no. 8206308, doi:10.1109/TMAG.2017.2700892.

[12] T. Matsuo and T. A. Lipo, "Rotor design optimization of synchronous reluctance machine," IEEE Trans. on Energy Convers., vol. 9, no. 2, pp. 359-365, June 1994, doi:10.1109/60.300136.

[13] R. Moghaddam and F. Gyllensten, "Novel High-Performance SynRM Design Method: An Easy Approach for A Complicated Rotor Topology," IEEE Trans. on Ind. Electron., vol. 61, no. 9, pp. 5058-5065, Sept. 2014, doi:10.1109/TIE.2013.2271601.

[14] C. Babetto, G. Bacco and N. Bianchi, "Synchronous Reluctance Machine Optimization for High-Speed Applications," IEEE Trans. on Energy Convers., vol. 33, no. 3, pp. 1266-1273, Sept. 2018, doi:10.1109/TEC.2018.2800536.

[15] Y. Wang, G. Bacco and N. Bianchi, "Geometry Analysis and Optimization of PM-Assisted Reluctance Motors," IEEE Trans. on Ind. Appl., vol. 53, no. 5, pp. 4338-4347, Sept.-Oct. 2017, doi:10.1109/TIA.2017.2702111.

[16] S. M. Taghavi and P. Pillay, "A Mechanically Robust Rotor With Transverse Laminations for a Wide-Speed-Range Synchronous Reluctance Traction Motor," IEEE Trans. on Ind. Appl., vol. 51, no. 6, pp. 4404-4414, Nov.-Dec. 2015, doi:10.1109/TIA.2015.2445819

[17] A. Credo, G. Fabri, M. Villani and M. Popescu, "High Speed Synchronous Reluctance Motor for Electric Vehicles: a Focus on Rotor Mechanical Design," in Proc. of IEEE IEMDC'19, May 2019, pp. 165-171, doi:10.1109/IEMDC.2019.8785083.

[18] V. B. Honsinger, "The inductances Ld and Lq of reluctance machines," IEEE Trans Power App. Syst., vol. 90, no. l, pp. 298-304, Jan./Feb. 1971, doi: 10.1109/TPAS.1971.293005.

[19] D. A. Staton, W. L. Soong and T. J. E. Miller, "Unified theory of torque production in switched reluctance and synchronous reluctance motors," IEEE Trans. Ind. Appl., vol. 31, no. 2, pp. 329-337, March-April 1995, doi: 10.1109/28.370281.

[20] A. E. Fitzgerald and J. R. Kingsley, "Electrical Machinery", 6th ed. New York: McGraw-Hill, 2003.

[21] S. Panda and R. K. Keshri, "Design and Analysis of Synchronous Reluctance Motor for Light Electric Vehicle Application," in Proc. of IEEE IECON'18, Oct. 2018, pp. 2021–2025, doi:10.1109/IECON.2018.8591404.

[22] A. Vagati, G. Franceschini, I. Marongiu and G. P. Troglia, "Design criteria of high performance synchronous reluctance motors," in Proc. Conf. Rec. IEEE Ind. Appl. Soc. Annu. Meeting, Oct. 1992, pp. 66–73, doi:10.1109/IAS.1992.244463.

[23] M. Ruba et al., "Synchronous reluctance machine geometry optimisation through a genetic algorithm based technique," IET Electric Power Applications, vol. 12, no. 3, pp. 431-438, 3 2018, doi:10.1049/iet-epa.2017.0455.